Quantitative Description of Genomic Evolution of Olfactory Receptors

Sk. S. Hassan, P. Pal Choudhury, B. S. Daya Sagar, *Senior Member, IEEE,* S. Chakraborty, R. Guha and A. Goswami

***Abstract*—We investigate how evolutionary network is associated among Human, Chimpanzee and Mouse with regards to their genomic information. We provide a quantitative description of genomic evolution through indexes based on fractal and mathematical morphology. We have considered olfactory receptors for our case study. These olfactory receptors do function in different species with the subtle differences in between the structures of DNA sequences. Those subtle differences along with common genomic information could be unraveled through computed quantitative indexes.**

***Index Terms*— Olfactory Receptor, Fractal dimension, Morphological Skeleton, Bifurcation Dimension.**

I. Introduction

HUMANS recognize a gigantic variety of chemicals as having distinctive odors. Odor perception initiates in the nose, where odorants are detected by a large family of olfactory receptors (ORs) [1]. ORs are the basis for the sense of smell, and they constitute the largest gene super family in the human genome. There are about 30,000 to 40,000 protein-coding genes in the human genome [2]. However, the genes are more complex, with more alternative splicing generation of larger number of protein products. To gain insight into the mechanisms underlying odor perception, the amount of complexities and the quantitative differences in different genes of various species, we provide a quantitative description of three OR sequences taken from Human, Mouse and Chimpanzee. Many experiments have been conducted in different research labs across the globe but to the best of our knowledge, not much work has been done to decipher the quantitative content of genome. We believe the geometry and morphology of the DNA structure are important aspects in studying their functions. We follow popular techniques to decipher quantitative aspects of DNA through fractals and mathematical morphology [3, 4, 5, 6, 7 and 8] that are employed to study many problems encountered in various branches of science and technology including the domain of biology. In this paper, we captured the evolutionary connections among ORs with the help of their quantitative descriptions.

Date used and Data representation: Date are acquired from the Yale University database (ORDB: http://senselab.med.yale.edu/ordb/). This data are represented in text form which we further represented in spatial form and is coded in 2-bit (4 color). Each nucleotide is assigned with unique color such that spatially represented data show from different colors. OR for Chimpanzee is shown in Fig. 1a. Similar representations are made for other two species Human and Mouse. We consider the olfactory receptors (Ors) OR1D2, CONTIG3463.6-1888, GA_x5J8B7W3YLM-7051808 of Human, Chimpanzee and Mouse respectively for our case study [9]. It is noted that we had selected the OR OR1D2 from HORDE database and it was blasted in the NCBI database (http://blast.ncbi.nlm.nih.gov/Blast.cgi) to get highly similar OR sequences in Chimpanzee and Mouse and we found that the CONTIG3463.6-1888, GA_x5J8B7W3YLM-7051808 of Chimpanzee and Mouse respectively.

Morphology can provide boundaries of images, their skeletons, convex hulls, watershed for segmentation and many more [5 and 6]. The primary aim is to extract important features from image data, from which a quantitative significant understanding of the topology of the image can be drawn. Mathematical morphology has shown promising results dealing with biological phenomena and in bioinformatics [10, 11, 12, 13, 14, 15, 16 and 17]. Fractal techniques have been employed by researchers in characterizing genomic signals and DNA sequences [18 and 19]. We employed various techniques from these two theories of geometric relevance to derive various characteristics of ORs to verify whether there exists any commonly shared physical mechanism.

This paper is organized as follows. Section II provides basic details of mathematical morphology [20, 21] and fractal geometry [22, 23 and 24]. Section III provides the methods to estimate quantitative indexes. Experimental results and concluding remarks are given in Sections IV and V.

Sk. S. Hassan is with Indian Statistical Institute, Kolkata, 700108 India (corresponding author to provide phone: +919609174055; e-mail: sarimif@isical.ac.in).

P. Pal Choudhury is with Indian Statistical Institute, Kolkata, 700108 India (e-mail: pabitra@isical.ac.in).

B. S. Daya Sagar, is with Indian Statistical Institute, Bangalore, India. (email: bsdsagar@isibang.ac.in).

S. Chakraborty is with Indian Statistical Institute, Kolkata, 700108 India (e-mail: shantanav89@gmail.com).

R. Guha is with Indian Statistical Institute, Kolkata, 700108 India (e-mail: ranita1990@gmail.com).

A. Goswami is with Indian Statistical Institute, Kolkata, 700108 India (e-mail: agoswami@isical.ac.in).

II. Some Basics and Fundamentals

Quantitative description for ORs is done through some basics of mathematical morphology and fractal geometry. For better understanding, the basic morphological transformations are stated below. Further, these two fields of mathematics are explained in the next subsections.

A. Basics on Mathematical Morphology

Mathematical Morphology based on axiomatic set theory and more relevantly lattice theory, has gained popularity out of its obvious uses in the field of image analysis which provides a quantitative description of geometrical structures. In this article, we apply certain morphological transformations essentially to gain the spatial distribution of different nucleotides in DNA sequence templates. To perform these analyses, two fundamental morphological transformations employed include morphological erosion (to shrink) and morphological dilation (to expand) as explained in equations (1) and (2).

$$\left(X \ominus \hat{B}\right) = \{x: B_x \subseteq X\} = \bigcap_{b \in B} X_{-b} \ldots\ldots (1)$$

$$\left(X \oplus \hat{B}\right) = \{x: B_x \cap X\} = \bigcup_{b \in B} X_{-b} \ldots\ldots (2)$$

where $B \neq \hat{B}$.

For further descriptions reader may refer to [7, 8, 9, and 10]. Also we have emphasized some other quantitative parameters as reviewed from a well written article [19].

B. Basics on Fractal

The precise definition of "Fractal" according to Benoit Mandelbrot is, a set for which the Hausdroff Besicovitch dimension strictly exceeds the topological dimension [22]. One of the fundamental fractal parameters is 'Fractal Dimension'. There are several methods like box counting method, perimeter area dimension method and so on to compute fractal dimension of an object. In this paper we follow box counting method and is computed through well known software called BENOIT™.

One of the important parameters is 'succolarity' which is really meant for the continuous density of the image / fractal [23].

III. Methods and Model Description

Quantitative measures such as poly-string mean and poly-string standard deviation, fractal dimension, succolarity index, bifurcation dimension, morphological entropy employed in our study from the field of Fractal Geometry and Mathematical Morphology. The method to estimate these measures are explained on a model (Fig.-1a) with specification.

A. Model Decomposition and Representation

Let a DNA sequence be in the form of four-letter (ATGC) nucleotides sequence (Fig. 1a). Such sequence shown in Fig. 1a is converted as a function (Fig. 1b) depicting colors RED, BLUE, GREEN, and YELLOW respectively for A, T, G, and C. In other words, such a function $f(x,y)$ corresponds to the above model DNA sequences be two bit pixel image. This allows $f(x,y)$ having maximum of 4 colors, i.e. $0 \leq f(x,y) \leq 3$.

ATGACAGGATTGAAAAATAAGAATTACACATTATTCCTTTA
ACATTGAGTTTCCCAGCTTTGAAGTAGCTGAAATAATTATA
TCGCATAAAAACTTTGTTATATTTTTCACTTTCTTATTTTC
AAAAATTATAAAATTGGGTGTAAGACATTCTTAATTCTAAG
AAAATGTTGATTTTGCTTATCTTCATGTTTTTATTCAATTA
AGGACTTTTGGTAAACATTTGCTGGTGTTAATGTTAAAAGA
GAGTTGGGGAAATGGATGGCATGGGGCTCTGGGAAGACTCC
TAGATAAACACTTTAAGAGGCT

(a)

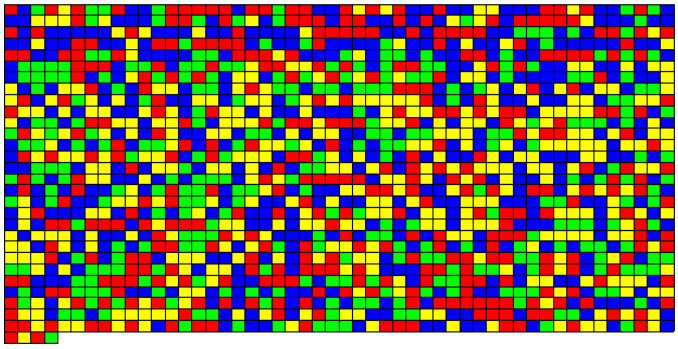

(b)

Fig. 1. (a) a DNA sequence, and (b) function generated by proper color coding for ATGC of CONTIG3463.6-1888

Threshold decomposition: We decomposed the four colored image $f(x,y)$ into four binary images (Fig. 2a-d) for Chimpanzee (Fig. 1b), through the threshold decomposition function defined as:

$$f^i(x,y) = 1\,;\; z = i : i = 0, 1, 2 \; and \; 3.$$

$$= 0\,; z \neq i$$

Those decomposed binary images for chimpanzee are denoted as ${f_{CH}}^A, {f_{CH}}^T, {f_{CH}}^G \; and \; {f_{CH}}^C$. Such binary images for species Human and mouse are denoted respectively as ${f_H}^A, {f_H}^T, {f_H}^G \; and \; {f_H}^C$ (for human) and ${f_M}^A, {f_M}^T, {f_M}^G \; and \; {f_M}^C$ (for mouse)

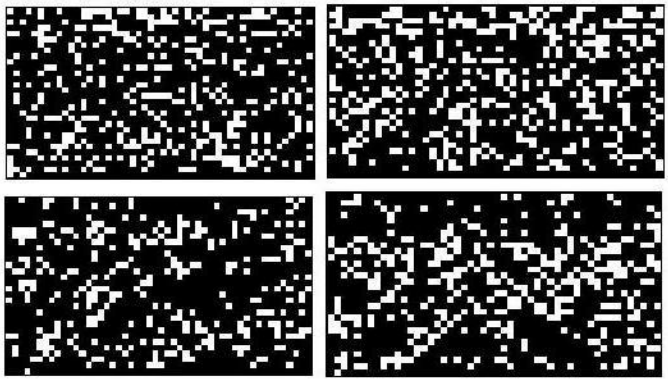

Fig. 2: Threshold decomposed binary images of ORs of Chimpanzee (Black and white denote complimentary space and one of the ATGC). (a) A (b) T (c) G, and (d) C.

Skeleton Decomposition: Morphological skeletons (Fig. 3a-d) for threshold decomposed binary images of ORs of Chimpanzee (CONTIG3463.6-1888) shown in Fig. 2a-d are obtained according to (3).

$$SK(X) = [(X \ominus nB)(X \ominus nB) \text{ O B}] \ldots\ldots (3)$$

where B is a structuring element that is symmetric about the origin, and $nB = B \oplus B \oplus B \ldots \oplus B(n\ times)$.

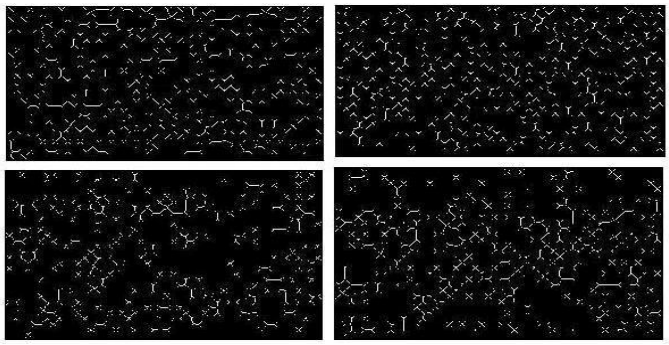

Fig. 3. Skeletons of OR Chimpanzee

Density and intricacy of the skeleton for those decomposed binary images depend upon the frequency of occurrence of nucleotide chosen as threshold and their spatial distribution. The intricacy of the skeleton is proportional to the heterogeneity in the spatial distribution of the skeleton.

Binary Representation: We have considered a DNA as a one dimensional nucleotide sequence, and is represented as a map such that $T(A) = 00;\ T(T) = 11,\ T(C) = 01\ and\ T(G) = 10$. This mapping yields a DNA sequence in a a binary string format. A portion of such a binary string is shown below of some fixed size (twice of the DNA sequence length).

00111000010010100011111000000000001100001000001111
00010001001111001111010111111100000100111110001011
11110101010010011111111000001011001001111000000011
00001111001100110110010011000000000001111111101111
00110011111111110100011111110111110011111111010000
00000011110011000000001111101010111011000010000100
1111011111…..(some more 0, 1 are there in the string).

B. Methods for different measures

The techniques employed to derive indexes are from the fields of mathematical morphology and fractal geometry further to retrieve geometric characteristics in quantitative manner. In particular, we employed skeletonization and granulometries from mathematical morphology and fractal dimension, Hurst exponent, succolority measures from fractal geometry to derive six quantitative indexes that also include poly-string mean and standard deviation. Data represented in spatial form enables rich geometric characteristics.

Poly-String Mean and Standard Deviation (A classification method): Let total number of poly-strings of different size $k_1, k_2, k_3, k_4 \ldots . k_n$ of nucleotide 'N' are $m_1, m_2, m_3, m_4 \ldots . m_n$. Then poly-string mean $\left({P_m}^N\right)$ and poly-string standard deviation $({P_{SD}}^N)$ of N are defined as

$${P_m}^N = \frac{\sum_{i=1:n} m_i k_i}{\sum_{1:n} m_i} \text{ and } {P_{SD}}^N = \sqrt{\frac{1}{n}\sum_{i=1}^{n} m_i (k_i - {P_m}^N)^2}$$

After calculating four nucleotides poly string mean and standard deviation will get a strict ordering relation among the ${P_M}^N$ and ${P_{SD}}^N$. We can classify any DNA sequence according to the order of ${P_M}^N$ and ${P_{SD}}^N$.

Fractal Dimension of Indicator Matrix: We have plotted a DNA sequences in two axes and defined a indicator map $f: \{X, Y\} \rightarrow \{0, 1\}\ as$

$$f(X, Y) = 0\ if\ Y \neq X$$

$$= 1\ otherwise$$

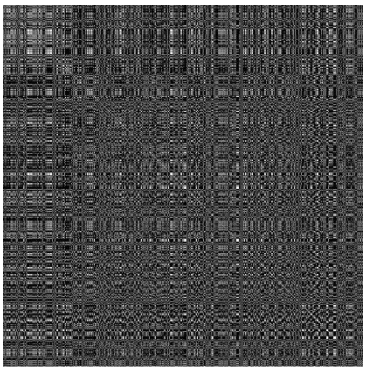

Fig-4: Indicator matrix

Then we have calculated the box-counting dimension of the indicator matrix on using the *Benoit* software.

The box counting dimension method computes the number of cells required to entirely cover an object, with grids of cells of varying size. Practically, this is performed by superimposing regular grids over an object and by counting the number of

occupied cells. The logarithm of N(r), the number of occupied cells, versus the logarithm of 1/r, where r is the size of one cell, gives a line whose gradient corresponds to the box dimension [22]. The box dimension is defined as the exponent D associated with the relation $D = \frac{\log N(r)}{\log 1/r}$.

Hurst Exponent: The Hurst exponent [19] is used as a measure of the long term memory of time series, i.e. the autocorrelation of the time series. Where a value of $0 < H < 0.5$ indicates a time series with negative autocorrelation (e.g. a decrease between values will probably be followed by an increase), and a value of $0.5 < H < 1$ indicates a time series with positive autocorrelation (e.g. an increase between values will probably be followed by another increase). A value of $H=0.5$ indicates a true random walk, where it is equally likely that a decrease or an increase will follow from any particular value with higher values indicating a smoother trend and less roughness.

Let a string $x = \{x_i\}_{i=1\ to\ n}$, defines the following entities regarding the sequence as:

$$m_{x,n} = \frac{1}{n}\sum_{i=1}^{n} x_i$$

$$X(i,n) = \sum_{j=1}^{i}\{x_j - m_{x,n}\}$$

$$R(n) = \max X(i,n) - \min X(i,n) : 1 \le i \le n$$

$$S(n) = \sqrt{\frac{1}{n}\sum_{i=1}^{n}(x_i - m_{x,n})^2}$$

Then Hurst Exponent (H) is defined as $\left(\frac{n}{2}\right)^H = \frac{R(n)}{S(n)}$

In our case 'n' denotes the length of the binary strings corresponding to each DNA sequence and x_i are the binary digits of the strings. The Hurst exponent varies between 0 and 1. In our present study we can calculate the Hurst exponent for any binary string (as shown in III (A)).

Succolarity index: The degree of percolation of an image (how much a given fluid can flow through this image) can be measured through Succolarity, a fractal parameter. The succolarity of a binary image is defined below [22]

$$\sigma(BS(k), dir) = \frac{\sum_{k=1}^{n} OP(BS(k)) \times PR(BS(k), pc)}{\sum_{k=1}^{n} PR(BS(k), pc)},$$

where 'dir' denotes direction, BS(n) where n is the number of possible divisions of a binary image in boxes. The occupation percentage (OP) is defined as, for each box size, k, then the sum of the multiplications of the OP (BS(k)), where k is a number from 1 to n, by the pressure PR(BS(k),pc), where pc is the position on x or y of the centroid of the box on the scale of pressure) applied to the box are calculated. The detailed of the method can be found in [23]. Therefore for any binary decomposed images of $f(x,y)$, the succolarity can be obtained.

Morphometric Dimension: It is conspicuous that the skeletal networks (Fig. 3a-d) decomposed from threshold decomposed binary images (Fig. 2a-d) of ORs of Chimpanzee possess branching pattern. The open-ended segments in the skeleton network are designated as first order segments, and second order segments begin from the point where two first order segments join, and where two second order segments join a third order segment begins, and so on. If any lower order segment joins to a higher order segment, higher order designation is maintained. We designated the skeletal networks according to this segment ordering scheme, and we computed order-wise number of skeletal segments $N(\omega)$, and order-wise mean lengths of skeletal segments $L(\omega)$. By using these two quantities we estimated bifurcation (R_B) and mean length (R_L) ratios of order-designated segments as follows:

$$R_B == \frac{N(\omega,\Omega)}{N(\omega+1,\Omega)} \text{ and } R_L = \frac{L(\omega+1,\Omega)}{L(\omega,\Omega)}$$

Further, we estimated fractal dimension using the ratio of logarithms of these topological quantities (i.e.$\frac{\log R_L}{\log R_B}$). For the four skeletal networks decomposed from four threshold decomposed binary images (Fig. 3a-d), the estimated fractal dimensions are given in Fig. 7.

Morphological Entropy: Here let us see how A, T, G, C are spatially distributed in a DNA sequence. We need to calculate the area (# of blocks) of the images by successive morphological opening on $f_H{}^A, f_H{}^T, f_H{}^G, f_H{}^C, f_M{}^A, f_M{}^T, f_M{}^G, f_M{}^C$ *and* $f_{CH}{}^A, f_{CH}{}^T, f_{CH}{}^G$. We then calculate the probability through the probability density function:

$$P_n(X|B) = \frac{\mathcal{A}[X - (X \circ nB)]}{\mathcal{A}[X]}$$

where X is the decomposed images of $f(x,y)$. The *Morphological Entropy* (ME) is defined as $-\sum_{n=0}^{N} P_n \log P_n$ where N is defined as

$$N = \text{Min}\{n: [X - (X \circ nB)] \neq \varphi, [X - (X \circ (n+1)B)] = \varphi\}.$$

IV. RESULTS AND DISCUSSIONS

We estimated six quantities namely poly-string mean, poly-string standard deviation, Hurst exponent, fractal dimension, succolarity index and morphological entropy for ORs of Human, Mouse and Chimpanzee--OR1D2, CONTIG3463.6-1888, GA_x5J8B7W3YLM-7052533-7051808 respectively for our case study. We could observe significant connections through the quantitative measures, described in the section-III.

A. Evolutionary Connection of ORs of Mouse and Chimpanzee with Human ORs

We have classified all the human ORs based on classification methodology on the poly-string mean and standard deviation as proposed in [15]. Using the similar methodology we have classified OR1D2 (Human), GA_x5J8B7W3YLM-7052533-7051808 (Mouse) and CONTIG3463.6-1888 (Chimpanzee),

and the results are shown in Table-I. We have also computed the Hurst exponent for all the three sequences. In the information that follows, we provided the indexes computed according 6 different methods of geometric relevance.

TABLE 1 EVOLUTIONARY CONNECTION OF ORS WITH HUMAN OBSERVED THROUGH HURST EXPONENT

Olfactory Receptors	***Class According to Poly-String Mean/SD***	***Hurst Exponent (H)***	***Maps to OR W.r.to H***
OR1D2	CGTA/CGAT	0.598911	OR1D2
GA_x5J8B7W3YLM-7052533-7051808	GCTA/GCAT	0.645594	OR4D2
CONTIG3463.6-1888	CGAT/ACTG	0.539152	OR3A3

The Mouse OR (GA_x5J8B7W3YLM-7052533-7051808) maps to a human OR OR4D2 based on classification and closest Hurst exponent. But it is to be noted that GA_x5J8B7W3YLM-7052533-7051808 is more similar to OR1D2. But as far as Hurst exponent is concerned (amount of long range correlation in the sequence), the mouse OR maps to OR4D2. It is our strong conviction that OR4D2 and OR1D2 are structurally similar in sequence despite the fact that they belong to different families as per HORDE qualitative classification. Also we discovered that mouse and human ORs are significantly similar in structure and in function.

The Chimpanzee OR (CONTIG3463.6-1888) maps to a human OR OR3A3 according to the classification (Table 1). Although OR3A3 and OR1D2 belong to different families but with respect to evolution in connection with Chimpanzee OR CONTIG3463.6-1888, they are structurally almost same as per quantification shown above.

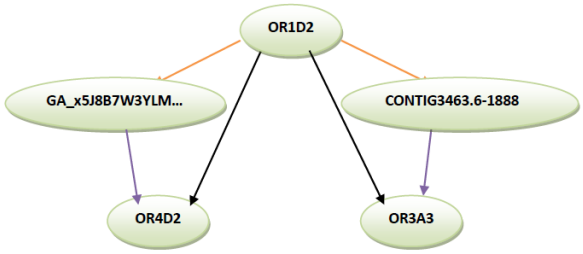

Fig-5: Evolutionary connect ion among Human, Mouse and Chimpanzee ORs

It is obvious from Fig. 5 that OR1D2, GA_x5J8B7W3YLM-7052533-7051808 and CONTIG3463.6-1888 are most similar to OR4D2 and OR3A3 further qualifying the strong evolutionary connection. Hence through biological evolution CONTIG3463.6-1888 and GA_x5J8B7W3YLM-7052533-7051808 are updated as OR3A3 and OR4D2 respectively.

B. Fractal and Morphological Quantification of ORs

The estimated fractal dimensions (Fig. II) of Indicator matrices for all three sequences—OR1D2 CONTIG3463.6-1888, GA_x5J8B7W3YLM-7052533-7051808 respectively include 1.77687, 1.81916 and 1.82963. We observed that fractal dimensions of ORs of Chimpanzee and Mouse are significantly similar. Through genomic evolution they got updated into OR1D2 in human. The fractal dimension of OR1D2 is reduced by a small amount 0.04 i.e. through genomic evolution amount of complexity or disorderliness got decremented.

C. Results on Succolarity

By treating a DNA sequence as a texture of four disjoint templates of A, T, C and G, these succolarity indexes are estimated. Estimated succolarity indexes for three ORs' DNA sequences of Human, Mouse and Chimpanzee are shown (Fig. 6).

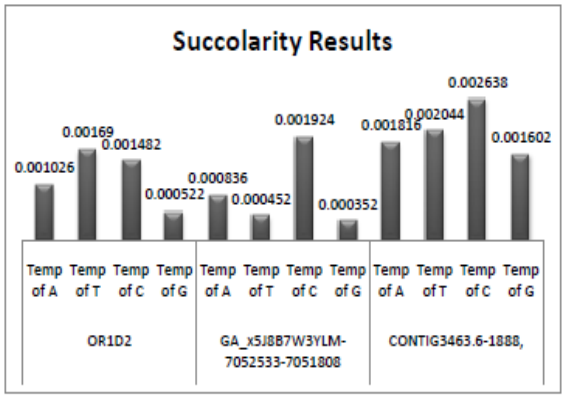

Figure-6: Succolarity index of each template of ORs of the three considered species.

The succolarity of all the textures of A, T, C, and G are significantly similar for ORs of Mouse and Chimpanzee. Whereas in the case of Human OR OR1D2 are less than that of other two ORs. It is obvious that over genomic evolution the succolarity (amount of continuous density) in sequence structure in Human OR is smaller than the other similar sequences of Mouse and Chimpanzee.

D. Results on Morphometric Dimension of Skeleton

Morphometry-based fractal d*imensions* for four skeletons are computed and found significant similarity among the three (Fig. 7).

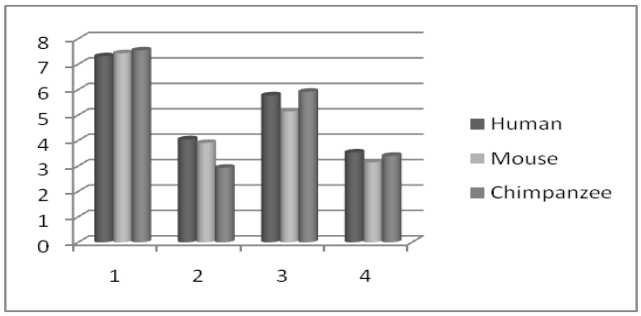

Fig.-7: Histogram of Morphometric Dimensions.

In Fig. 7, it is apparent that they do not follow a strict order. We believe this parameter provide a distinction between the functions of ORs.

E. Results on Morphological Entropy (Spatial Distribution)

The area in pixel units (cardinality) of successive openings on the decomposed images of each of the DNA 4 color images are depicted in Table 2.

TABLE 2: AREA OVER SUCCESSIVE OPENING

Decomposed ??? enitity	***Area (in pixel units) retained after opening cycles (0 - 6)***						
	0	*1*	*2*	*3*	*4*	*5*	*6*
$f_H{}^A$	170	26	6	1	1	0	
$f_H{}^C$	189	67	15	4	2	0	
$f_H{}^G$	147	39	8	2	0		
$f_H{}^T$	214	36	8	1	0		
$f_M{}^A$	120	19	5	2	0		
$f_M{}^C$	165	52	7	2	1	0	
$f_M{}^G$	101	30	6	2	0		
$f_M{}^T$	172	34	6	2	0		
$f_{CH}{}^A$	278	59	21	8	5	1	0
$f_{CH}{}^C$	256	81	17	5	3	0	
$f_{CH}{}^G$	221	59	14	2	0		
$f_{CH}{}^T$	317	79	20	6	2	0	

The morphological entropy values are calculated for all the decomposed images of $f(x,y)$, shown in Fig. 8, by considering the sequentially decreasing areal extent with increasing opening cycles.

H: Hurst exponent
$P_n(X|B)$: Probability density function
$\sigma(BS(k), dir)$: Succolarity
R_L, R_B : Mean length and bifurcation ratio.

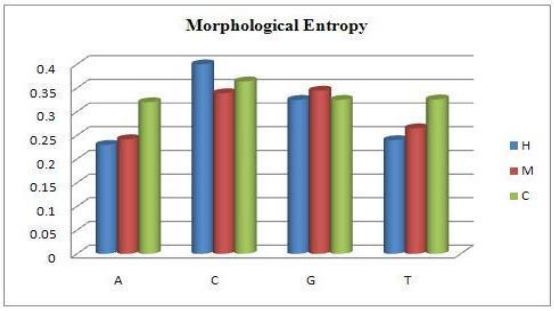

Fig.-8: ME of decomposed images of $f(x,y)$

From Fig. 8, it is noticed that the morphological entropy of the decomposed images of A and T for all the species are significantly similar. In other words we can say that the spatial distribution of A and T in three sequences are almost same due to the fact of homologue relationship among them. But the spatial distribution of C and G are different from others individually, and it is our strong conviction that this differentiation makes them distinct species-wise.

V. CONCLUSION AND FUTURE ENDEAVORS

We have shown an evolutionary connection among Human, Mouse and Chimpanzee ORs by quantitative means. These sequences have very close sequential similarity but they do different in different species due to their intricate details of the structures in the DNA sequence. Those intricate details are illustrated here. In our further study, we deal with similar characterization via fractal and mathematical morphology-based indexes to provide a quantitative classification with some more details about all the ORs of Human, Chimpanzee and Mouse.

ACKNOWLEDGMENT

The authors are grateful to Prof. Jean Serra, Emeritus Professor, ESIEE-Engineering, University Paris-Est, Former Director of Centre for Mathematical Morphology, France for his kind advice and suggestions and also express their gratitude to Mr. Pratap Vardhan for his technical help in writing programs.

APPENDIX: LIST OF NOTATIONS AND SYMBOLS

OR: Olfactory Receptor
$\ominus$: Morphological erosion
$\oplus$: Morphological dilation
$\hat{B}$: Bilateral reflexion of the structuring element B.
A: Adenine, C: Cytosine, G: Guanine, T: Thiamine
$f(x,y)$: Four color image of a DNA
$f_{CH}{}^A, f_{CH}{}^T, f_{CH}{}^G, f_{CH}{}^C$: Binary decomposition of $f_{CH}(x,y)$
$f^i(x,y)$: Decomposition function
$SK(X)$: Morphological skeleton of f.
O: Morphological opening
$P_m{}^N$: Poly-string mean, $P_{SD}{}^N$: Poly-string SD.
$m_{x,n}$: Mean of $x = \{x_i\}_{i=1\ to\ n}$

REFERENCES

[1] B. Malnic and PA Godfrey, "The olfactory receptor gene family," *Proc. Natl. Acad. Sc*, Vol. 101 pp. 2584-2589 2004.

[2] P Kitts, EV Koonin, I Korf, D Kulp and D Lancet, "Initial sequencing and analysis of the human genome", *Nature*, Vol. 409, pp. 860-921, 2001.

[3] G Matheron and J Serra, "History of Mathematical Morphology*", http://cmm.ensmp.fr/~serra/pdf/birth_of_mm.pdf*

[4] B. S. Daya Sagar "Fractal relations of a morphological skeleton", *Chaos, Solitons & Fractals*, Vol. 7, no. 11, pp. 1871-1879.

[5] B. S. Daya Sagar, et al, "Morphometric relations of fractal-skeletal based channel network model", "*Discrete Dynamics in Nature and Society"*, Vol 2, no. 2, pp. 77-92. 1998

[6] P. Radhakrishnan, B. S. Daya Sagar, and Teo Lay Lian, "Estimation of fractal dimension through morphological decomposition", *Chaos, Solitons & Fractals*, Vol 21, no. 3, pp. 563-572. 2004

[7] B. S. Daya Sagar and Tay Lea Tien, " Allometric power-law relationships in a Hortinian fractal digital elevation model," *Geophysical Research Letters*, Vol. 31, no. 6, L06501.

[8] Shih and Mitchell "Threshold Decomposition of Gray -Scale Morphology into Binary Morphology", *IEEE transactions on Pattern Analysis and Machine Intelligence* Vol. 11, No. 1. Pp. 31-42, 1989.

[9] Yoav Gilad, Orna Man and Gustavo Glusman, "A comparison of the human and chimpanzee olfactory receptor gene repertoires," *Genome Res*. Vol. 15 no.2 pp. 224-30, 2005.

[10] J. G. Venkateswaran, B. Song, and T. Kahveci, "A Tool for Finding Distant Structural Similarities," *IEEE/ACM Transactions on Computational Biology and Bioinformatics*," Vol: 8 no.3 pp: 819-831, 2011.

[11] G. Cardona, M. Llabres, and F. Rossello, "Comparison of Galled Trees," *"IEEE/ACM Transactions on Computational Biology and Bioinformatics"* Vol. 8 no: 2 pp: 410-427, 2011

[12] J. Stoye and R. Wittler, "A Unified Approach for Reconstructing Ancient Gene Clusters," *"IEEE/ACM Transactions on Computational Biology and Bioinformatics"* Vol. 6 no: 3 pp. 387-400, 2009

[13] Q. Zhu, Z. Adam and V. Choi, "Generalized Gene Adjacencies, Graph Bandwidth, and Clusters in Yeast Evolution," *"IEEE/ACM Transactions on Computational Biology and Bioinformatics"*Vol. 6 no: 2 pp. 213-220, 2009

[14] R. Boscolo, C. L James and P. V. Roychowdhury, "An information theoretic exploratory method for learning patterns of conditional gene coexpression from microarray data." *"IEEE/ACM Transactions on Computational Biology and Bioinformatics"* Vol. 5 no: 1 pp. 15-24, 2008

[15] A. Phaedra; B. N. Kreiswirth, and N. Steve, "Typing Staphylococcus aureus using the spa gene and novel distance measures," *"IEEE/ACM Transactions on Computational Biology and Bioinformatics"* Vol. 4 no. 4 pp: 693-704, 2007

[16] M. A. Alekseyev and P. A. Pevzner, "Colored de Bruijn graphs and the genome halving problem," *"IEEE/ACM Transactions on Computational Biology and Bioinformatics"* Vol. 4 no. 1 pp. 98-107, 2007

[17] O. Abul, R. Alhajj and F. Polat, "A powerful approach for effective finding of significantly differentially expressed genes," *"IEEE/ACM Transactions on Computational Biology and Bioinformatics"* Vol. 3 no. 3 pp: 220-231, 2006.

[18] J. Serra, "Image Analysis and Mathematical Morphology", *Academic Press, Inc.* Orlando, FL, USA ©1983 ISBN: 0126372403. 1982.

[19] C. Carlo, "Fractals and Hidden Symmetries in DNA*", Mathematical Problems in Engineering* Vol. 2010, Article ID 507056.

[20] P. P. Choudhury, S.S. Hassan, S. Sahoo and B. K. Nayak, "Carry *Value Transformation (CVT): It's Application in Fractal formation", Advance Computing Conference*, pp. 971 – 976, 978-ISBN: 1-4244-2927-1, IEEE. 2009.

[21] P. Choudhury, S.S. Hassan, S. Sahoo and B. K. Nayak, "Act of CVT and EVT In the Formation of Number-Theoretic Fractals", *International Journal of Computer Cognition*, Vol 9, No. 1, pp. 1-8 2011.

[22] B. B. Mandelbrot, The fractal geometry of nature. New York, ISBN 0-7167-1186-9, 1982.

[23] R. H. C. de Melo and A. Conci, "Succolarity: Defining a Method to calculate this Fractal Measure," **ISBN:** 978-80-227-2856-0 , pp. 291 – 294, 2008

[24] Yu Zu-Guo, "Fractals in DNA sequence analysis*", Chinese Physics,* Vol 11, no. 12, pp.1313-1318, 2002.